JACS
JOURNAL OF THE AMERICAN CHEMICAL SOCIETY
pubs.acs.org/JACS
Article

Correlating Li-Ion Solvation Structures and Electrode Potential Temperature Coefficients

Hansen Wang,[$] Sang Cheol Kim,[$] Tomás Rojas,[$] Yangying Zhu, Yanbin Li, Lin Ma, Kang Xu, Anh T. Ngo,* and Yi Cui*

Cite This: https://dx.doi.org/10.1021/jacs.0c10587
Read Online
ACCESS | Metrics & More | Article Recommendations | Supporting Information

ABSTRACT: Temperature coefficients (TCs) for either electrochemical cell voltages or potentials of individual electrodes have been widely utilized to study the thermal safety and cathode/anode phase changes of lithium (Li)-ion batteries. However, the fundamental significance of single electrode potential TCs is little known. In this work, we discover that the Li-ion desolvation process during Li deposition/intercalation is accompanied by considerable entropy change, which significantly contributes to the measured Li/Li$^+$ electrode potential TCs. To explore this phenomenon, we compare the Li/Li$^+$ electrode potential TCs in a series of electrolyte formulations, where the interaction between Li-ion and solvent molecules occurs at varying strength as a function of both solvent and anion species as well as salt concentrations. As a result, we establish correlations between electrode potential TCs and Li-ion solvation structures and further verify them by *ab initio* molecular dynamics simulations. We show that measurements of Li/Li$^+$ electrode potential TCs provide valuable knowledge regarding the Li-ion solvation environments and could serve as a screening tool when designing future electrolytes for Li-ion/Li metal batteries.

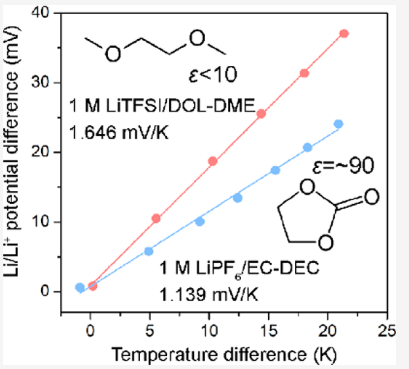

INTRODUCTION

Temperature affects both kinetics and thermodynamics of electrochemical processes in a battery. Kinetically, variations in temperature could significantly change the rates of ion transport in the bulk electrolytes and charge-transfer at interfaces, which eventually affect important properties including power delivery and cycling performances.[1] From a thermodynamics perspective, temperature is known to dictate the equilibrium voltage of an electrochemical cell,[2] and this has been utilized for waste-heat harvesting.[2−4] Temperature coefficient (TC) α quantifies this temperature dependency of the cell voltage, which is proportional to the entropy change of the full-cell reaction

$$\alpha = \frac{\partial E}{\partial T} = -\frac{1}{nF}\frac{\partial \Delta G}{\partial T} = \frac{\Delta S}{nF} \quad (1)$$

where E is the equilibrium cell voltage, T is the temperature, n is the number of electrons transferred in the reaction, F is Faraday's constant, and ΔG and ΔS are the Gibbs free energy and entropy change of the full-cell reaction. Similarly, TC can also be defined for a single electrode (half-cell reaction).[5] Under such definitions, a full cell TC also represents the difference in the TCs of the two electrodes

$$\frac{\partial E}{\partial T} = \frac{\partial \varphi_c}{\partial T} - \frac{\partial \varphi_a}{\partial T} \quad (2)$$

where φ_c and φ_a are the equilibrium cathode and anode potentials, respectively.

For lithium (Li)-ion batteries, TCs have mostly been measured for full cells under isothermal conditions, with the focus placed on determining the reversible heat generated from the batteries,[6−11] screening cathode-anode combinations to enhance thermal safety,[10,12] or detecting the special phase changes of the cathode/anode materials.[11−16] However, these studies usually neglect the determination of the TCs for individual electrodes, so a fundamental understanding about the physical origin of single electrode potential TCs remains unknown. In particular, Li-ion solvation/desolvation is an indispensable process in the half-cell reactions on both electrodes, yet its correlation to the single electrode potential TC cannot be reflected in full cell measurements due to the isothermal conditions. A recent study by Swiderska-Mocek et al. described the single electrode potential TC for several Li-ion battery electrodes[17] but stopped short of exploring their molecular origins.

Typically, the following half-cell reactions happen on a Li metal or a Li-ion host electrode

$$Solvated\ Li^+ + e^- \rightarrow Li^0 + Released\ solvents/anions \quad (3)$$

Received: October 5, 2020

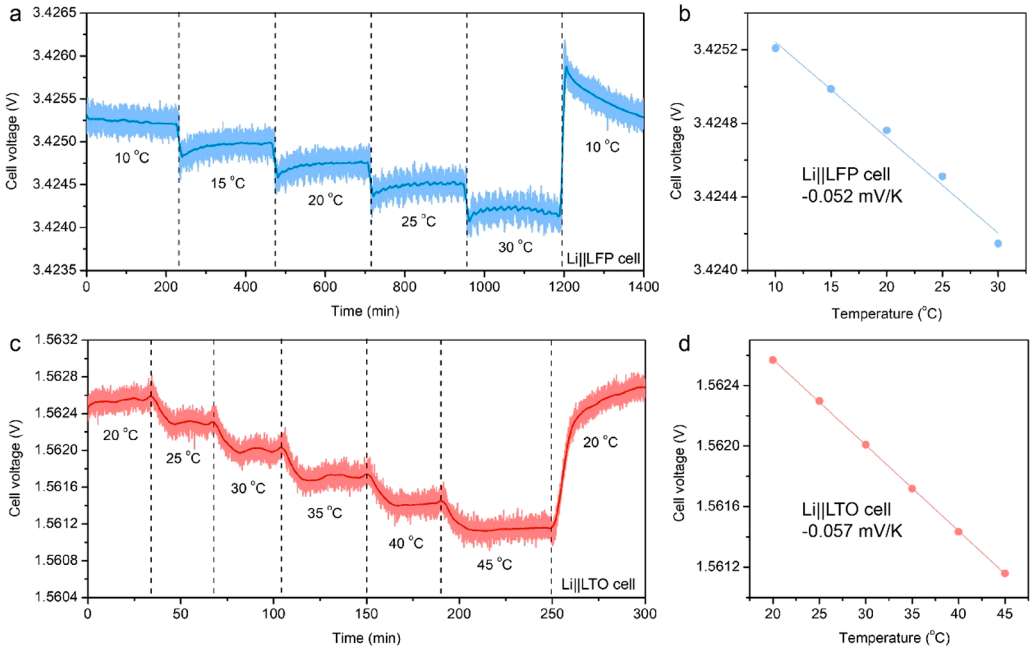

Figure 1. (a) Isothermal measurement of a Li||LFP coin cell (50% SOC) voltage under varied temperatures and (b) corresponding fitting result for the full cell voltage TC. (c) Isothermal measurement of a Li||LTO coin cell (50% SOC) voltage under varied temperatures and (d) corresponding fitting result for the full cell voltage TC.

$$Solvated\ Li^+ + e^- + host \rightarrow Li^+/host + Released\ solvents/anions \quad (4)$$

where the host represents either cathode or anode, whose lithiation mechanism can be either intercalation into lattice interstitial or via conversion-reaction process. The release of free solvent molecules/anions from a solvated Li-ion during its desolvation process inevitably leads to a considerable increase in the system entropy. Such desolvation process universally exists in the redox reaction of every Li metal or Li-ion battery electrode. Therefore, it should contribute significantly to the TCs measured for single electrode potentials.[5,17] Furthermore, changes of the electrolyte composition, such as solvents, anions or salt concentration, are known to affect Li-ion solvation structures, which subsequently alter the number of molecules released during desolvation, and should induce corresponding change in the TC. In fact, it has been observed that the TC for a Li metal electrode varies significantly in different electrolytes,[18] yet no attempt has been made to rationalize its origin at molecular level.

In this work, we first measure the full-cell/electrode TCs and confirm that the change in electrolyte composition induces pronounced variations in the Li/Li^+ electrode potential TC. Then we systematically study the changes in Li/Li^+ electrode potential TCs against electrolyte concentrations, electrolyte solvents, and Li salts. Together with *ab initio* molecular dynamics (AIMD) simulations, we successfully establish the correlation between TCs and Li-ion solvation environments. Knowledge of such correlation could possibly serve as a guideline to the design and screening of future electrolytes for Li-ion/Li metal batteries.

RESULTS

Full Cell Voltage TC. Full cell voltage TCs are measured under isothermal conditions for either Li||lithium iron phosphate (LFP) or Li||lithium titanate (LTO) coin cells using 1 M lithium hexafluorophosphate ($LiPF_6$)/ethylene carbonate (EC)-diethylene carbonate (DEC) (v/v = 1:1) as the electrolyte. Specifically, a Li||LFP or Li||LTO cell is cycled to 50% state of charge (SOC), after formation cycles under C/10, and then placed in an environmental chamber. Open circuit voltage (OCV) is measured for the cell under a sequence of temperatures. The OCV evolution is recorded for both the Li|| LFP and Li||LTO cell (Figure 1a, c). Both cells show decreasing OCV with increasing temperatures, indicating negative TCs. The TC results are achieved by fitting the equilibrium state OCV against temperature, which is shown in Figure 1b, d and Table 1.

Table 1. Isothermal Full Cell TC Results

	TC (mV/K)
Li||LFP	−0.052
Li||LTO	−0.057

The results of negative but near zero TCs for both cells are consistent with previous reports,[16] indicating that Li metal has a higher single electrode potential TC than both LFP and LTO electrodes at 50% SOC, yet the difference is very small. The lower single electrode potential TC of LFP/LTO originates from the smaller entropy change correlated with the addition of Li into the solid state electrode materials. Being measured at isothermal conditions, full cell TCs are only related to the entropy change of the solid-state electrode materials, while providing no information on the individual electrode TCs and their molecular origins. In particular, contributions from the electrolyte are completely negated since the entropy change from the Li-ion solvation and desolvation processes, which happen simultaneously at the anode and cathode, cancel each other out. Therefore, nonisothermal measurements on the electrode TCs are needed.

Electrolyte Dependence of Electrode Potential TCs. Nonisothermal measurements are performed for Li metal

https://dx.doi.org/10.1021/jacs.0c10587
J. Am. Chem. Soc. XXXX, XXX, XXX−XXX

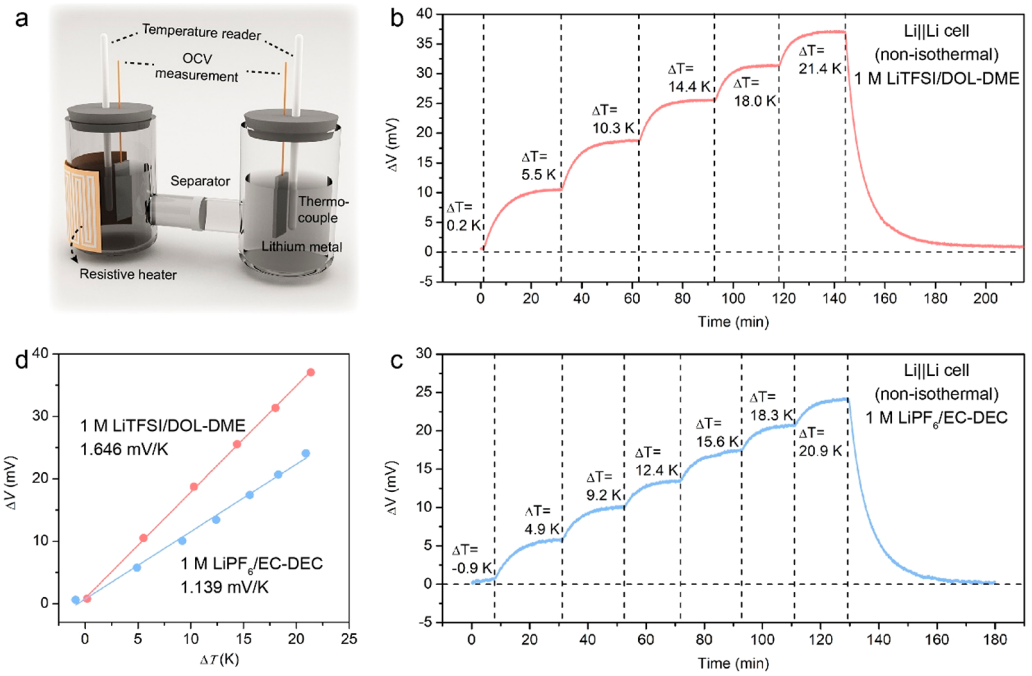

Figure 2. (a) Schematic of the nonisothermal measurement H-cell configuration. (b) Evolution of the Li||Li H-cell OCV under a sequence of temperature differences using 1 M LiTFSI/DOL-DME as the electrolyte. (c) Evolution of the Li||Li H-cell OCV under a sequence of temperature differences using 1 M $LiPF_6$/EC-DEC as the electrolyte. (d) Li/Li^+ electrode potential TC fitting results in the two electrolytes.

electrodes in an H-cell configuration (Figure 2a). Two Li metal electrodes are placed in the two chambers with thermocouples placed on their surfaces so that the OCV (ΔV) and temperature can be accurately measured. One of the chambers is wrapped with a resistive heater to create temperature differences (ΔT) between the two electrodes. OCV (ΔV) evolutions are recorded using 1 M lithium bis(trifluoromethanesulfonyl)imide (LiTFSI)/dioxolane (DOL)-dimethoxyethane (DME) (v/v = 1:1) and 1 M $LiPF_6$/EC-DEC (v/v = 1:1) electrolytes (Figure 2b,c). The TCs for Li/Li^+ can be achieved by fitting ΔV against ΔT at equilibrium states (Figure 2d and Figure S1). Here, we assume that the thermal diffusion potentials between the hot/cold electrolyte (Soret effect) and thermoelectric potentials between the hot/cold metallic wires (Thomson effect) are both negligible. This assumption is justified by the previously reported data revealing that the Soret and Thomson coefficients have values of 10−50 μV/K,[5,17,20] ~ 20−100 times smaller than the fitting results in our measurements (Figure 2d). Under this assumption, Li/Li^+ electrode potential has a TC of 1.646 mV/K in 1 M LiTFSI/DOL-DME and 1.139 mV/K in 1 M $LiPF_6$/EC-DEC. Furthermore, with the Li/Li^+ TCs and the full cell TCs measured above, single electrode potential TCs for other cathodes (LFO) and anodes (LTO, graphite) can also be calculated from eq 2 (Table 2). It can be observed that the single electrode TCs vary only slightly among different electrode materials in the same electrolyte; however, they are significantly affected by the different electrolyte compositions (Figure 2d). This indicates that the entropy contribution from the phase changes in the solid-state electrode materials likely contribute a minor portion to the half-reaction ΔS. On the contrary, the Li desolvation process, which exists in the half-reactions of all the electrodes measured, contributes significantly to the ΔS as well as single electrode potential TCs. This observation provides thermodynamic explanation to the earlier report that Li-ion desolvation presents the rate-determining-step in the charge-transfer process at interfaces.[21] A correlation between electrolyte compositions and single electrode potential TCs has hitherto never been proposed. Therefore, we further compare Li/Li^+ TCs in electrolytes with varying Li-ion solvation power by changing electrolyte species and concentrations.

Table 2. Single Electrode Potential TC Results in 1 M $LiPF_6$/EC-DEC Electrolyte

Electrode	TC (mV/K)
Li	1.139
Graphite (~80% SOC)	0.970[19]
LTO (~50% SOC)	1.082
LFP (~50% SOC)	1.087

Concentration Dependence of Electrode Potential TCs. Electrolyte concentration has been known to significantly impact the Li-ion solvation environment as well as battery performances.[22−24] Therefore, we anticipate that it must have a profound impact on the half reaction ΔS. We measure the Li/Li^+ electrode potential TCs and corresponding entropy changes (ΔS) in nonisothermal H-cells for LiTFSI/DOL-DME (v/v = 1:1) and $LiPF_6$/EC-DEC (v/v = 1:1) electrolytes with different concentrations (Figure S2 and Figure S3). The TC results can be observed in Figure 3 and Table 3. Completely different TC trends against concentrations are observed for the two electrolyte systems. For the ether-based LiTFSI/DOL-DME system, where the polydentate ethers tend to form tight solvation cages for Li-ion, Li/Li^+ TC decreases from 1.870 to 1.023 mV/K as the electrolyte concentration increases from 0.2 to 5 M. In contrast, Li/Li^+ TCs maintain ~1.1 mV/K under different concentrations in the carbonated-based $LiPF_6$/EC-DEC system, where Li-ion is relatively free from its solvation sheath. This result indicates that the electrolyte solvent/salt species constitute the key parameter that determines the TC evolution against electrolyte concentrations. To resolve the

https://dx.doi.org/10.1021/jacs.0c10587
J. Am. Chem. Soc. XXXX, XXX, XXX−XXX

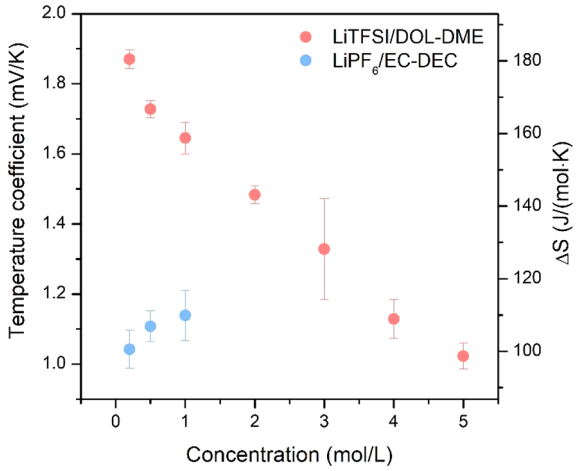

Figure 3. Li/Li$^+$ electrode potential TC under different concentrations of LiTFSI/DOL-DME and $LiPF_6$/EC-DEC systems.

correlation between the electrolyte composition and concentration-dependence of Li/Li$^+$ TCs, we resort to *ab initio* molecular dynamics (AIMD) simulations, which reveals the dynamics and energetics of the Li-ion solvation in different electrolytes.

AIMD Simulations. $LiPF_6$/EC-DEC and LiTFSI/DOL-DME electrolytes with concentrations of 0.5, 1, and 2 M are chosen for the AIMD simulations. First, we resolve the Li-ion solvation environments (Figure 4a,b, Figures S4a,b and S5a,b) at equilibrium states (last 1 ps of the simulations). To reveal the coordination structures between Li-ions and the solvents, the radial distribution function g(r) is also averaged among the structures of the last 20 ps of the simulations (Figure 4c,d, Figures S4c,d and S5c,d). It can be observed that in $LiPF_6$/EC-DEC electrolytes, EC molecules dominate the Li-ion solvation shells at all concentrations, with one oxygen atom per EC molecule coordinating with a Li-ion. In LiTFSI/DOL-DME electrolytes, DME molecules dominate the Li-ion first solvation shells at all concentrations, with two oxygen atoms per DME molecule (under the *gauche* conformation) coordinating with a Li-ion. Our simulations results under 1 M conditions are consistent with previous simulation[25,26] as well as experimental reports,[27−29] while those under 0.5 and 2 M conditions contribute to further understandings of how Li-ion solvation evolves at different electrolyte concentrations.

On the basis of the Li-ion solvation structure results, we also average the binding energy (BE) between the first Li-ion solvation shell and the remaining molecules in the electrolytes (Figure 4e) from 5 images extracted from the last 20 ps of each simulation with 4 ps intervals (Figure 4a,b, Figures S4a,b, S5a,b, and S6−S11). We define this binding energy by subtracting the energy of the first solvation shell and the remaining electrolyte from the total energy of the entire system

$$BE = E_{system} - (E_{1^{st}\ solvation\ shell} + E_{remaining\ electrolyte}) \quad (5)$$

This binding energy can be a proxy for desolvation entropy. Higher BE signifies greater interaction between the first solvation shell and the bulk electrolyte and the formation of a larger solvation structure beyond the first solvation shell. This leads to a greater number of molecules involved in solvation, which can lead to an increased entropy change upon desolvation.

It can be observed that this binding energy is much larger in value for the LiTFSI/DOL-DME system than the $LiPF_6$/EC-DEC system. We attribute the phenomenon to the significant difference in the dielectric constants (ε) between carbonate and ether molecules. ε for EC molecule has been reported to be ~90,[30−33] while ε for DOL and DME molecules are both below 10.[26,34] Having the Li-ions surrounded by a layer of higher dielectric constant molecules like EC would shield the charge of the Li-ions, leading to weaker electrostatic interactions between the Li-ion to the solvent molecules beyond the first solvation shell. The opposite scenario happens for the DOL-DME system, where the solvent shielding effect is weak and the Li-ion still has strong interactions with the solvent molecules beyond first the first solvation shell.

Correlating Li-Ion Solvation to Li/Li$^+$ Electrode Potential TCs. On the basis of the AIMD simulation results, we propose that the relationship between the Li-ion solvation structures in the selected electrolytes and their corresponding Li/Li$^+$ TC is as follows:

First, Li/Li$^+$ has higher electrode potential TCs in LiTFSI/DOL-DME than $LiPF_6$/EC-DEC under the same concentrations because

1. A DME molecule chelates onto a Li-ion with two oxygen atoms under the *gauche* conformation, resulting in no rotational freedom in the DME molecule (Figure 4b). In contrast, an EC molecule binds to a Li-ion with only one oxygen atom, so that its ring can rotate freely (Figure 4a). This possibly leads to lower system entropy for the half reaction reactants (solvated Li-ions, left side of eq 3) in the LiTFSI/DOL-DME electrolytes.
2. Due to the strong screening effect of EC molecules than DOL/DME molecules, the Li-ion residing in the first solvation shell has much weaker interactions with outer solvent molecules in the $LiPF_6$/EC-DEC electrolytes (Figure 4e). This indicates that in the $LiPF_6$/EC-DEC

Table 3. Non-Isothermal Li|Li H-Cell TC Results for Electrolytes with Different Concentrations

	Conc. (mol/L)	Li/Li$^+$ TC (mV/K)				Avg. TC (mV/K)	Avg. ΔS (J/(mol·K))
$LiPF_6$/EC-DEC	0.2	1.003	1.019	1.104		1.042	100.54
	0.5	1.051	1.158	1.115	1.108	1.118	106.91
	1.0	1.118	1.218	1.080		1.139	109.86
LiTFSI/DOL-DME	0.2	1.872	1.851	1.907	1.851	1.870	180.45
	0.5	1.728	1.761	1.722	1.701	1.728	166.73
	1.0	1.703	1.662	1.612	1.606	1.646	158.79
	2.0	1.515	1.469	1.491	1.458	1.483	143.11
	3.0	1.444	1.461	1.226	1.182	1.328	128.16
	4.0	1.156	1.195	1.085	1.080	1.129	108.93
	5.0	1.012	1.077	0.994	1.007	1.023	98.66

https://dx.doi.org/10.1021/jacs.0c10587
J. Am. Chem. Soc. XXXX, XXX, XXX−XXX

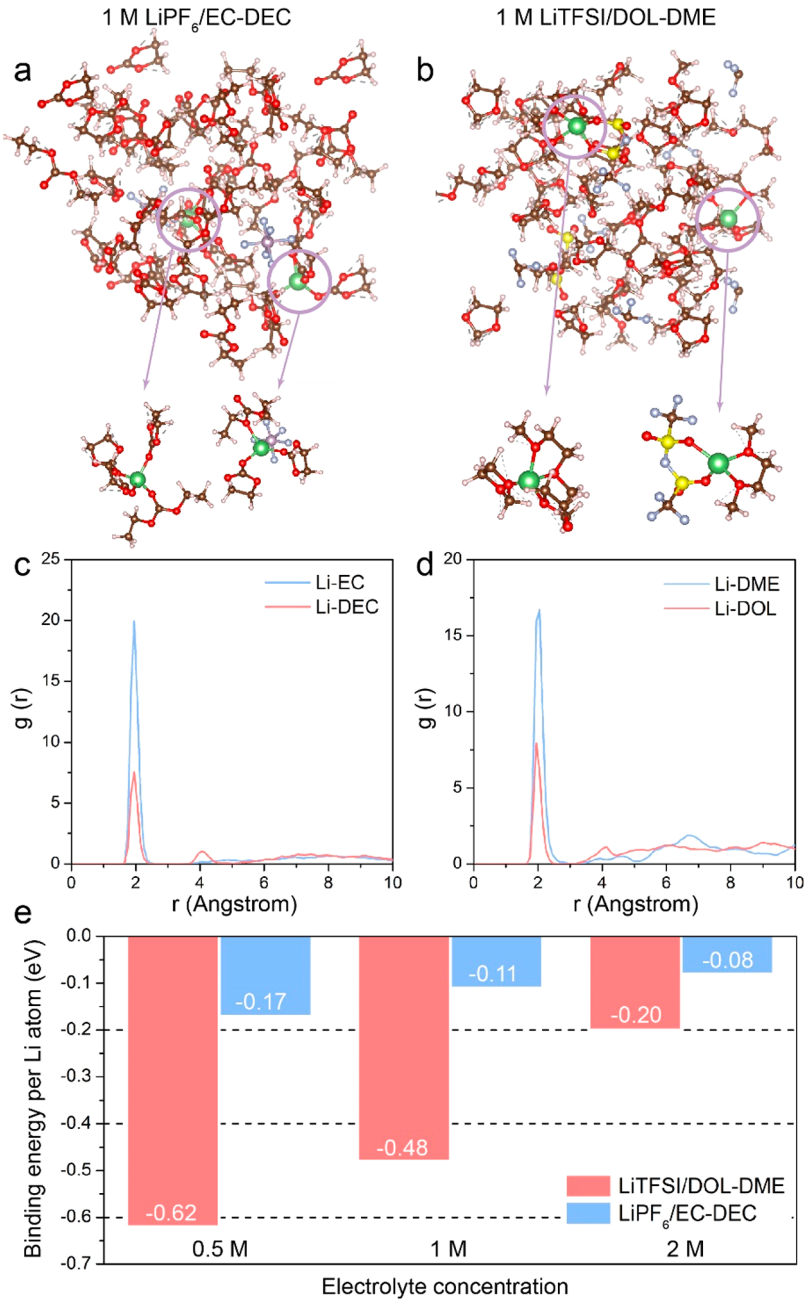

Figure 4. (a) Li-ion solvation environment in 1 M $LiPF_6$/EC-DEC electrolyte. The spheres of color green, red, silver, purple, pink, and brown represent Li, O, F, P, H, and C atoms, respectively. First solvation shells of the Li-ions are further depicted at the bottom. (b) Li-ion solvation environment in 1 M LiTFSI/DOL-DME electrolyte. The spheres of color green, red, silver, yellow, pink, and brown represent Li, O, F, S, H, and C atoms, respectively. First solvation shells of the Li-ions are further depicted at the bottom. (c) The radial distribution function g(r) of the O atoms on EC/DEC molecules around Li-ions in 1 M $LiPF_6$/EC-DEC electrolyte. (d) The radial distribution function g(r) of O atoms on DOL/DME molecules around Li-ions in 1 M LiTFSI/DOL-DME electrolyte. (e) Binding energy between the Li-ion first solvation shell and the remaining molecules for $LiPF_6$/EC-DEC and LiTFSI/DOL-DME electrolytes with different concentrations.

electrolytes, a Li-ion almost only binds with the solvent and anion molecules in the first shell, while in the LiTFSI/DOL-DME electrolytes, the electrostatic field of a Li-ion possibly reaches the solvent molecules beyond the first solvation shell and instead will have multilayers of solvation. Therefore, many more solvent molecules coordinated with the Li-ion would be released in the LiTFSI/DOL-DME electrolytes during the desolvation process, leading to higher entropy of the half reaction products (right side of eq 3).

With a combination of these two factors, the Li/Li^+ redox reaction (eq 3) should have considerably higher ΔS in the LiTFSI/DOL-DME than in the $LiPF_6$/EC-DEC electrolyte under the same concentration, as reflected in the higher electrode potential TCs in the LiTFSI/DOL-DME system.

Second, we corroborate the different TC evolution trends against concentrations in the two systems.

1. In the LiTFSI/DOL-DME system, binding energy per Li-ion between first solvation shells and the remaining molecules decreases significantly in value as the electro-

https://dx.doi.org/10.1021/jacs.0c10587
J. Am. Chem. Soc. XXXX, XXX, XXX−XXX

lyte concentration increases (from −0.62 at 0.5 M to −0.20 at 2 M; Figure 4e). This is intuitive because at higher concentrations, the solvent to Li-ion ratio decreases so that fewer solvent molecules are available in the outer shells to interact with a Li-ion. Correspondingly, at higher concentrations, fewer solvent molecules per Li-ion would be released during desolvation, indicating lower ΔS for the half reaction (eq 3), namely, lower TCs for the Li/Li$^+$ electrode potential (Figure 3).

2. A similar effect also exists in the LiPF$_6$/EC-DEC system. However, it is much less significant in extent due to the strong charge screening effect of the EC molecules. A Li-ion intrinsically has very weak interactions with outer solvent molecules, so that the decrease in this binding energy at a higher electrolyte concentration is minimal (from −0.17 at 0.5 M to −0.08 at 2 M; Figure 4e). As a result, the change in half reaction (eq 3) ΔS is negligible so that the measured Li/Li$^+$ TCs remain similar across different electrolyte concentrations (Figure 3).

Li Salt Dependence of Electrode Potential TCs. Finally, TCs are compared for electrolytes based on various Li salts of different Li-ion mobilities and dissociation constants,[35] which are critical parameters in affecting the performances of Li-ion batteries.[32] In particular, we anticipate that their different dissociation constants should have direct impacts on the system entropy. Therefore, TCs for the electrolytes with 1 M of LiPF$_6$, lithium perchlorate (LiClO$_4$), LiTFSI, lithium bis(fluorosulfonyl)imide (LiFSI), lithium bis(oxalato)borate (LiBOB), and lithium trifluoromethanesulfonate (LiOTf) in EC-DEC (v/v = 1:1) were compared (Figure S12 and Figure 5).

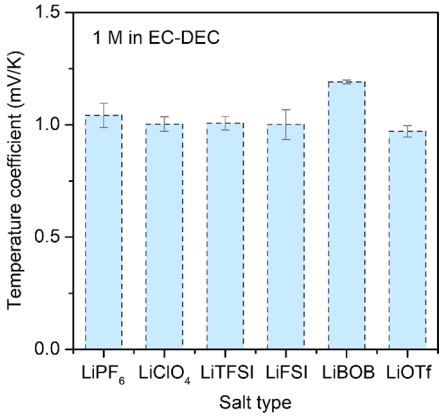

Figure 5. Li/Li$^+$ electrode potential TCs in EC-DEC electrolytes with 1 M Li salt with different anions.

No obvious trend can be established between the Li salt dissociation constants and Li/Li$^+$ TC (Table 4). Even for Li salts with very low dissociation constants such as LiBOB and LiOTf,[32] the TCs are still measured to be ∼1.1 mV/K. We attribute this to the following reasons.

1. Under 1 M concentration, solvent to anion ratio is large (11.8 solvent molecules to 1 anion). The number of anions is possibly too low to have pronounced impact on the half reaction (eq 3) ΔS.
2. Although the percentage of associated ion pairs is affected by the Li salt dissociation constants, the total number of solvent molecules/anions interacting with a Li-ion in the first solvation shell usually does not change.[35] The half reaction (eq 3) ΔS is therefore affected insignificantly.

Nevertheless, we believe the Li salt dissociation constants possibly impact the Li/Li$^+$ TCs to a considerable extent under high concentration conditions, which deserves further study in the future.

Table 4. Non-Isothermal Li||Li H-Cell TC Results for EC-DEC with 1 M Different Li Salts

Li salt	Li/Li$^+$ TC (mV/K)		Avg. TC (mV/K)	Avg. ΔS (J/(mol·K))
LiClO$_4$	1.026	0.981	1.004	96.82
LiTFSI	0.986	1.029	1.008	97.21
LiFSI	1.048	0.954	1.001	96.58
LiBOB	1.197	1.185	1.191	114.91
LiOTf	0.989	0.953	0.971	93.69

CONCLUSIONS

We systematically study the effects of electrolyte solvents, salts, and concentrations on the Li/Li$^+$ electrode potential TCs, and establish the direct correlation between Li/Li$^+$ electrode potential TCs and the Li-ion solvation structures. We observe much larger TCs in LiTFSI/DOL-DME than those in LiPF$_6$/EC-DEC electrolytes at the same concentration. Furthermore, TCs in the LiTFSI/DOL-DME electrolytes decrease with increasing electrolyte concentrations, while TCs in the LiPF$_6$/EC-DEC electrolytes almost remain unchanged. Utilizing AIMD simulations, we resolve the Li-ion solvation structures and energetics in different electrolyte systems, which elucidates the physical origins of the experimental observations. In particular, the coordination configurations between the Li-ion and the solvent molecules as well as the solvent dielectric constants serve as the key factors leading to the different TC results. We also observe that Li salts have a weak impact on the Li/Li$^+$ TC under 1 M, but more pronounced impacts might arise at increased concentrations. Our findings exhibit that the measurement of single electrode potential TCs could provide valuable information on the solvation environments in the corresponding electrolytes. Combined with other characterizations tools, it could serve as a useful descriptor to screen new electrolytes for various battery systems.

EXPERIMENTAL SECTION

Isothermal Full Cell TC Measurement. LFP or LTO electrodes are first made through a doctor blade-casting method. The electrodes were cut in to 1 cm^2 disks and transferred into an Ar-filled glovebox. Coin cells were prepared by pairing Li metal disks with either LFP or LTO electrodes, with 1 M LiPF$_6$/EC-DEC (Gotion) as the electrolyte and PP/PE/PP (Celgard 2325) as the separator. The Li||LFP or Li|| LTO coin cells were first cycled under C/10 for two cycles and then charged or discharged to 50% SOC. Afterward, the cells were transferred into an environmental chamber (BTU-133, ESPEC North America) with high-precision (±0.1 °C) temperature control. Programs were written for the coin cells to experience a sequence of temperatures (1−2 h at each temperature to reach equilibrium state), and the OCV of the cells were recorded with a potentiostat (VMP3, BioLogic) throughout the experiments.

Nonisothermal Li||Li H-Cell TC Measurement. The H-cell was placed inside an Ar-filled glovebox with oxygen and a water level below 0.1 ppm. Two identical Li metal electrodes which were electrically connected to copper clips were placed in the two chambers. Different electrolytes (reported in the main text) were added, which wetted the electrodes but not the copper clips to avoid corrosion that could introduce artifacts in the measurement. A PP/PE/PP separator

https://dx.doi.org/10.1021/jacs.0c10587
J. Am. Chem. Soc. XXXX, XXX, XXX−XXX

(Celgard 2325) was inserted in the bridge of the H-cell to reduce fluid mixing while allowing ion transport. A thermocouple (Omega, HSTC-TT-K-24S-36) was installed in each half cell adjacent to the electrode surface to measure the temperature of the electrolyte/electrode interface. A Kapton heater was wrapped around one side of the H-cell to provide uniform heating. During the measurement, the heating power was adjusted via a DC Keithley power source. For each heating power set point, temperatures were recorded with a temperature scanner (Omega, DP1001AM). Open circuit voltage between the two electrodes was recorded using a potentiostat (VMP3, BioLogic).

AIMD Simulations. The AIMD calculations were performed using the density functional theory (DFT) framework, specifically the generalized gradient approximation. The projector-augmented wave (PAW) formalism was employed as implemented in the Vienna Ab initio Simulation Package (VASP).[36−38] We simulated the electrolytes using a computational supercell (14 × 14 × 14 Å) that is composed of about 350 atoms with periodic boundary conditions over all directions.

We employed the PAW pseudopotentials supplied by VASP and the exchange-correlation functional developed by Perdew−Burke−Ernzerhof (PBE)[39] was used. The plane-wave energy cutoff was set at 600 eV, and the Brillouin zone was sampled at the Γ point. The initial configuration of the electrolytes was prepared by setting the EC, DEC, and $LiPF_6$ molecules at random positions and orientations; the concentrations of each compound are determined by the experimental volume ratios and analogously for the DOL, DME, and LiTFSI system. Each system was equilibrated at 298.15 K in the canonical ensemble (NVT) for around 100 ps with a time step of 1 fs. The Nose-Hoover thermostat[40] was used to impose the condition of constant temperature.

■ ASSOCIATED CONTENT

Supporting Information

The Supporting Information is available free of charge at https://pubs.acs.org/doi/10.1021/jacs.0c10587.

Impacts of interphases on voltage measurements, fitting results, simulated solvation environments, and radial distribution functions for different electrolyte formulations (PDF)

■ AUTHOR INFORMATION

Corresponding Authors

Yi Cui − *Department of Materials Science and Engineering, Stanford University, Stanford, California 94305, United States; Stanford Institute for Materials and Energy Sciences, SLAC National Accelerator Laboratory, Menlo Park, California 94025, United States;* orcid.org/0000-0002-6103-6352; Email: yicui@stanford.edu

Anh T. Ngo − *Materials Science Division, Argonne National Laboratory, Lemont, Illinois 60439, United States; Department of Chemical Engineering, University of Illinois at Chicago, Chicago, Illinois 60607, United States;* Email: ango@anl.gov

Authors

Hansen Wang − *Department of Materials Science and Engineering, Stanford University, Stanford, California 94305, United States;* orcid.org/0000-0002-6738-1659

Sang Cheol Kim − *Department of Materials Science and Engineering, Stanford University, Stanford, California 94305, United States*

Tomás Rojas − *Materials Science Division, Argonne National Laboratory, Lemont, Illinois 60439, United States; Department of Chemical Engineering, University of Illinois at Chicago, Chicago, Illinois 60607, United States*

Yangying Zhu − *Department of Materials Science and Engineering, Stanford University, Stanford, California 94305, United States*

Yanbin Li − *Department of Materials Science and Engineering, Stanford University, Stanford, California 94305, United States;* orcid.org/0000-0002-5285-8602

Lin Ma − *Energy & Biotechnology Division, Sensors and Electron Devices Directorate, US Army Research Laboratory, Adelphi, Maryland 20783, United States;* orcid.org/0000-0003-1183-1347

Kang Xu − *Energy & Biotechnology Division, Sensors and Electron Devices Directorate, US Army Research Laboratory, Adelphi, Maryland 20783, United States;* orcid.org/0000-0002-6946-8635

Complete contact information is available at: https://pubs.acs.org/10.1021/jacs.0c10587

Author Contributions

[$]These authors contributed equally.

Author Contributions

H.W., S.C.K., and T.R. contributed equally to this work.

Notes

The authors declare no competing financial interest.

■ ACKNOWLEDGMENTS

This work was supported by the Assistant Secretary for Energy Efficiency and Renewable Energy, Office of Vehicle Technologies of the US Department of Energy under the eXtreme Fast Charge Cell Evaluation of Li-ion batteries (XCEL) program (Grant: 34553). The authors acknowledge the computing resources provided on Bebop, a high-performance computing cluster operated by the Laboratory Computing Resource Center at Argonne National Laboratory.

■ REFERENCES

(1) Liu, Y.; Zhu, Y.; Cui, Y. Challenges and opportunities towards fast-charging battery materials. *Nat. Energy* **2019**, *4* (7), 540−550.

(2) Yang, Y.; Lee, S. W.; Ghasemi, H.; Loomis, J.; Li, X.; Kraemer, D.; Zheng, G.; Cui, Y.; Chen, G. Charging-free electrochemical system for harvesting low-grade thermal energy. *Proc. Natl. Acad. Sci. U. S. A.* **2014**, *111* (48), 17011.

(3) Lee, S. W.; Yang, Y.; Lee, H.-W.; Ghasemi, H.; Kraemer, D.; Chen, G.; Cui, Y. An electrochemical system for efficiently harvesting low-grade heat energy. *Nat. Commun.* **2014**, *5* (1), 3942.

(4) Gao, C.; Lee, S. W.; Yang, Y. Thermally Regenerative Electrochemical Cycle for Low-Grade Heat Harvesting. *ACS Energy Lett.* **2017**, *2* (10), 2326−2334.

(5) deBethune, A. J.; Licht, T. S.; Swendeman, N. The Temperature Coefficients of Electrode Potentials. *J. Electrochem. Soc.* **1959**, *106* (7), 616.

(6) Bazinski, S. J.; Wang, X. The Influence of Cell Temperature on the Entropic Coefficient of a Lithium Iron Phosphate (LFP) Pouch Cell. *J. Electrochem. Soc.* **2014**, *161* (1), A168−A175.

(7) Bang, H.; Yang, H.; Sun, Y. K.; Prakash, J. In Situ Studies of $Li_xMn_2O_4$ and $Li_xAl_{0.17}Mn_{1.83}O_{3.97}S_{0.03}$ Cathode by IMC. *J. Electrochem. Soc.* **2005**, *152* (2), A421.

(8) Lu, W.; Yang, H.; Prakash, J. Determination of the reversible and irreversible heats of $LiNi_{0.8}Co_{0.2}O_2$/mesocarbon microbead Li-ion cell reactions using isothermal microcalorimetery. *Electrochim. Acta* **2006**, *51* (7), 1322−1329.

(9) Onda, K.; Ohshima, T.; Nakayama, M.; Fukuda, K.; Araki, T. Thermal behavior of small lithium-ion battery during rapid charge and discharge cycles. *J. Power Sources* **2006**, *158* (1), 535−542.

(10) Viswanathan, V. V.; Choi, D.; Wang, D.; Xu, W.; Towne, S.; Williford, R. E.; Zhang, J.-G.; Liu, J.; Yang, Z. Effect of entropy change

of lithium intercalation in cathodes and anodes on Li-ion battery thermal management. *J. Power Sources* **2010**, *195* (11), 3720−3729.
(11) Yang, H.; Prakash, J. Determination of the Reversible and Irreversible Heats of a $LiNi_{0.8}Co_{0.15}Al_{0.05}O_2$/Natural Graphite Cell Using Electrochemical-Calorimetric Technique. *J. Electrochem. Soc.* **2004**, *151* (8), A1222.
(12) Lu, W.; Belharouak, I.; Park, S. H.; Sun, Y. K.; Amine, K. Isothermal calorimetry investigation of $Li_{1+x}Mn_{2-y}Al_zO_4$ spinel. *Electrochim. Acta* **2007**, *52* (19), 5837−5842.
(13) Takano, K.; Saito, Y.; Kanari, K.; Nozaki, K.; Kato, K.; Negishi, A.; Kato, T. Entropy change in lithium ion cells on charge and discharge. *J. Appl. Electrochem.* **2002**, *32* (3), 251−258.
(14) Al Hallaj, S.; Venkatachalapathy, R.; Prakash, J.; Selman, J. R. Entropy Changes Due to Structural Transformation in the Graphite Anode and Phase Change of the $LiCoO_2$ Cathode. *J. Electrochem. Soc.* **2000**, *147* (7), 2432.
(15) Maher, K.; Yazami, R. Effect of overcharge on entropy and enthalpy of lithium-ion batteries. *Electrochim. Acta* **2013**, *101*, 71−78.
(16) Zhang, W.; Jiang, L.; van Durmen, P.; Saadat, S.; Yazami, R. A Combined Thermodynamics & Computational Method to Assess Lithium Composition in Anode and Cathode of Lithium Ion Batteries. *Electrochim. Acta* **2016**, *214*, 56−67.
(17) Swiderska-Mocek, A.; Rudnicka, E.; Lewandowski, A. Temperature coefficients of Li-ion battery single electrode potentials and related entropy changes-revisited. *Phys. Chem. Chem. Phys.* **2019**, *21* (4), 2115−2120.
(18) Gritzner, G.; Lewandowski, A. Temperature coefficients of half-wave potentials and entropies of transfer of cations in aprotic solvents. *J. Chem. Soc., Faraday Trans.* **1991**, *87* (16), 2599−2602.
(19) Wang, H.; Zhu, Y.; Kim, S. C.; Pei, A.; Li, Y.; Boyle, D.; Zhang, Z.; Ye, Y.; Huang, W.; Liu, Y.; Xu, J.; Li, J.; Liu, F.; Cui, Y. Underpotential Lithium Plating on Graphite Anodes Caused by Temperature Heterogeneity. *Proc. Natl. Acad. Sci. U. S. A.* **2020**, *117* (47), 29453−29461.
(20) Yee, E. L.; Cave, R. J.; Guyer, K. L.; Tyma, P. D.; Weaver, M. J. A survey of ligand effects upon the reaction entropies of some transition metal redox couples. *J. Am. Chem. Soc.* **1979**, *101* (5), 1131−1137.
(21) Xu, K.; von Cresce, A.; Lee, U. Differentiating Contributions to "Ion Transfer" Barrier from Interphasial Resistance and Li^+ Desolvation at Electrolyte/Graphite Interface. *Langmuir* **2010**, *26* (13), 11538−11543.
(22) Qian, J.; Henderson, W. A.; Xu, W.; Bhattacharya, P.; Engelhard, M.; Borodin, O.; Zhang, J.-G. High rate and stable cycling of lithium metal anode. *Nat. Commun.* **2015**, *6* (1), 6362.
(23) Wang, H.; Cao, X.; Gu, H.; Liu, Y.; Li, Y.; Zhang, Z.; Huang, W.; Wang, H.; Wang, J.; Xu, W.; Zhang, J.-G.; Cui, Y. Improving Lithium Metal Composite Anodes with Seeding and Pillaring Effects of Silicon Nanoparticles. *ACS Nano* **2020**, *14* (4), 4601−4608.
(24) Wang, H.; Li, Y.; Li, Y.; Liu, Y.; Lin, D.; Zhu, C.; Chen, G.; Yang, A.; Yan, K.; Chen, H.; Zhu, Y.; Li, J.; Xie, J.; Xu, J.; Zhang, Z.; Vilá, R.; Pei, A.; Wang, K.; Cui, Y. Wrinkled Graphene Cages as Hosts for High-Capacity Li Metal Anodes Shown by Cryogenic Electron Microscopy. *Nano Lett.* **2019**, *19* (2), 1326−1335.
(25) Han, S. Structure and dynamics in the lithium solvation shell of nonaqueous electrolytes. *Sci. Rep.* **2019**, *9* (1), 5555.
(26) Park, C.; Kanduč, M.; Chudoba, R.; Ronneburg, A.; Risse, S.; Ballauff, M.; Dzubiella, J. Molecular simulations of electrolyte structure and dynamics in lithium-sulfur battery solvents. *J. Power Sources* **2018**, *373*, 70−78.
(27) Yang, L.; Xiao, A.; Lucht, B. L. Investigation of solvation in lithium ion battery electrolytes by NMR spectroscopy. *J. Mol. Liq.* **2010**, *154* (2), 131−133.
(28) Bogle, X.; Vazquez, R.; Greenbaum, S.; Cresce, A. v. W.; Xu, K. Understanding Li^+-Solvent Interaction in Nonaqueous Carbonate Electrolytes with ^{17}O NMR. *J. Phys. Chem. Lett.* **2013**, *4* (10), 1664−1668.
(29) Zhou, Y.; Su, M.; Yu, X.; Zhang, Y.; Wang, J.-G.; Ren, X.; Cao, R.; Xu, W.; Baer, D. R.; Du, Y.; Borodin, O.; Wang, Y.; Wang, X.-L.; Xu, K.; Xu, Z.; Wang, C.; Zhu, Z. Real-time mass spectrometric characterization of the solid-electrolyte interphase of a lithium-ion battery. *Nat. Nanotechnol.* **2020**, *15* (3), 224−230.
(30) Logan, E. R.; Tonita, E. M.; Gering, K. L.; Ma, L.; Bauer, M. K. G.; Li, J.; Beaulieu, L. Y.; Dahn, J. R. A Study of the Transport Properties of Ethylene Carbonate-Free Li Electrolytes. *J. Electrochem. Soc.* **2018**, *165* (3), A705−A716.
(31) Daniels, I. N.; Wang, Z.; Laird, B. B. Dielectric Properties of Organic Solvents in an Electric Field. *J. Phys. Chem. C* **2017**, *121* (2), 1025−1031.
(32) Xu, K. Nonaqueous Liquid Electrolytes for Lithium-Based Rechargeable Batteries. *Chem. Rev.* **2004**, *104* (10), 4303−4418.
(33) Xu, K. Electrolytes and Interphases in Li-Ion Batteries and Beyond. *Chem. Rev.* **2014**, *114* (23), 11503−11618.
(34) Rajput, N. N.; Murugesan, V.; Shin, Y.; Han, K. S.; Lau, K. C.; Chen, J.; Liu, J.; Curtiss, L. A.; Mueller, K. T.; Persson, K. A. Elucidating the Solvation Structure and Dynamics of Lithium Polysulfides Resulting from Competitive Salt and Solvent Interactions. *Chem. Mater.* **2017**, *29* (8), 3375−3379.
(35) Seo, D. M.; Borodin, O.; Han, S.-D.; Boyle, P. D.; Henderson, W. A. Electrolyte Solvation and Ionic Association II. Acetonitrile-Lithium Salt Mixtures: Highly Dissociated Salts. *J. Electrochem. Soc.* **2012**, *159* (9), A1489−A1500.
(36) Kresse, G.; Furthmüller, J. Efficient iterative schemes for ab initio total-energy calculations using a plane-wave basis set. *Phys. Rev. B: Condens. Matter Mater. Phys.* **1996**, *54* (16), 11169−11186.
(37) Kresse, G.; Joubert, D. From ultrasoft pseudopotentials to the projector augmented wave method. *Phys. Rev. B: Condens. Matter Mater. Phys.* **1999**, *59* (3), 1758−1775.
(38) Harl, J.; Schimka, L.; Kresse, G. Assessing the quality of the random phase approximation for lattice constants and atomization energies of solids. *Phys. Rev. B: Condens. Matter Mater. Phys.* **2010**, *81* (11), 115126.
(39) Perdew, J. P.; Burke, K.; Ernzerhof, M. Generalized gradient approximation made simple. *Phys. Rev. Lett.* **1996**, *77* (18), 3865−3868.
(40) Hoover, W. G. Canonical dynamics: equilibrium phase-space distributions. *Phys. Rev. A: At., Mol., Opt. Phys.* **1985**, *31* (3), 1695−1697.

https://dx.doi.org/10.1021/jacs.0c10587
J. Am. Chem. Soc. XXXX, XXX, XXX−XXX